

# “Scale oriented” embedded modeling of the North-Western Mediterranean in the frame of MFSTEP

C. Estournel<sup>1</sup>, F. Auclair<sup>1</sup>, M. Lux<sup>2</sup>, C. Nguyen<sup>1</sup>, and P. Marsaleix<sup>1</sup>

<sup>1</sup>Pôle d’Océanographie Côtière de Toulouse – Laboratoire d’Aérodologie, CNRS, Université de Toulouse, Toulouse, France

<sup>2</sup>Noveltis, Toulouse, France

Received: 30 October 2006 – Published in Ocean Sci. Discuss.: 12 February 2007

Revised: 16 February 2009 – Accepted: 15 March 2009 – Published: 27 April 2009

**Abstract.** An embedded forecasting system was developed for the North-Western Mediterranean at 3-km resolution. The system is based on the Symphonie hydrodynamic free surface model and on the variational initialization and forcing platform VIFOP. The regional model is initialized and forced at its open lateral boundaries by the MFS GCM and forced at the surface by the ALADIN numerical weather prediction model. Once a week, a five-day forecast is produced after a hindcast of seven days. This pre-modeling period of 7 days before beginning the forecast allows the development of the small scale features associated to the high resolution. The relevance of the 5-day forecast strategy has been examined by comparing the forecasted fields to hindcast fields (forced by meteorological and oceanic analyses) considered as a reference. Mismatches remain at a very low level indicating a good quality of the forecasted forcing fields and also possibly to the strong wind conditions which prevailed during the period. The embedded forecasts have been compared to the MFS observing system (SST and MedArgo) during 6 forecast cycles between September 2004 and February 2005. It was basically found that in the North-Western Mediterranean, the MFS basin-scale model and thus the regional model forecasts are characterized by large negative biases of salinity in the first 100 m under the surface leading thus to too light subsurface waters. The underestimation of temperature by the regional model just below the surface and its overestimation at 30m deep can be attributed to an overestimation of the turbulent mixing. The regional model allows to represent a number of processes especially those induced by the wind as coastal upwelling under stratified conditions, dense water formation over the Gulf of Lion shelf, deep mixing in the convection zone or influence on the Northern Current penetration in the Gulf of Lion.

## 1 Introduction

The regional modeling of the North-Western Mediterranean (NWM) is carried out in the frame of the Mediterranean Forecasting System (MFS). The MFS offered indeed an opportunity for both coastal and regional ocean modelers to progress from their classical “process oriented” studies to further “scale oriented” studies. The objective of scale oriented modeling is to explicitly model the linear and non-linear interactions of a large variety of processes occurring in a given range of space and time scales whereas, for long, process oriented modeling has focused on a limited number of processes neglecting their interactions with their dynamical environment. First of all, the second part of the MFS (Toward Environmental Predictions or MFSTEP) has been a successful observation laboratory of the Mediterranean over a large variety of physical scales. It also provides continuity and consolidates the objectives of the MFS Pilot Project (MFSPP) during which a clear embedded strategy had been proposed (Pinardi et al., 2003) and basin scale modeling had been carried out successfully (Demirov and Pinardi, 2002). To end up with, the coupling of physical and biochemical models has been proposed with a common forecasting objective.

To be successfully achieved, the regional modeling of the NWM has eventually been based not only on an observing system, but also on quality meteorological forecasts and analysis and on basin scale modeling. As dynamically opened systems, regional ocean modeling is indeed completely dependent on the quality of the various forcing. We thus clearly defend the idea that no small scale modeling strategy can be achieved without a strategy based on quality checks at every scale. As a consequence, we think that the regional modeler, far from being a modeler on its own, must be part of a cooperating team. At the opposite, basin scale modelers cannot pretend studying large scale circulation features without some precise quality checks along the



Correspondence to: C. Estournel  
(claude.estournel@aero.obs-mip.fr)

shelf breaks and the coasts. The MFS has grounded such believes in its basic strategy and is thus a source of scientific achievements.

Several scientific objectives were more specifically achieved during this project and are detailed in the present paper. First of all, by carrying out realistic long term regional modeling, the NWM dynamical processes could be studied in detail and validated based on several types of observations. As stated above, the MFS is also a unique opportunity to test and validate in an operational context the embedded modeling strategy proposed and developed in terms of open boundary conditions (Marsaleix et al., 2006) and initialization (Auclair et al., 2006). The regular distribution of forecasted fields<sup>1</sup> through the web in this “best effort context” implies both technical and scientific constrains. Scientifically first, this means that embedded models should not include any spin up period as even one-day forecast must be dynamically accurate. The embedded strategy has thus to be revisited and validated based on more demanding requirements. Technically, this means that the operational delivery has to be based on a computationally affordable and stringent numerical treatment and extensive validation.

In the following, the proposed regional modeling strategy is presented in Sect. 2. In Sect. 3, this strategy is evaluated by examining the development of small scales along the forecast cycle. Then the assessment of the forecasts is done by comparing the forecasts, the hindcasts and the GCM. The regional forecasts are then compared to dedicated observations while several physical processes are studied at well identified spatial scales in Sect. 4.

## 2 The NWM regional modeling system

### 2.1 Previous applications of hydrodynamic modeling in the North Western Mediterranean Sea

The MFS numerical strategy was not restricted to a single type of regional models as the POM (Princeton Ocean Model) and SYMPHONIE models have been implemented in specific regions. As far as the NWM is concerned, the modeling strategy was based not only on the SYMPHONIE model but also on the experience accumulated over years in this area. This experience covers indeed the modeling of the NWM oceanic circulation at *regional scale*, several studies of *the coastal dynamics* of the shelf of the Gulf of Lion, and eventually, at *smaller scales*, near-shore studies based on high resolution implementations of the hydrodynamic model.

At the regional scales, the oceanic circulation is principally characterized by the Liguro-Provençal-Catalan (LPC) current (or Northern Current). This current is highly constrained by the shelf break slope. As the continental shelf is rather narrow in the NWM Sea, the Northern current tends to

stick to the coast, except in the Gulf of Lion where the continental shelf is much larger. In this latter case, the Northern current flows mainly above the shelf break slope, about 100km offshore in the region of the Gulf of Lion, but secondary currents can flow onto the continental shelf, as shown by Petrenko et al. (2005). Auclair et al. (2001) studied this process from a numerical point of view. As far as short time scales are concerned (a critical issue since the MFSTEP regional forecasts do not extend over one week), they showed that the unbalance of the initial state, resulting from inconsistencies between the interpolated Mediterranean basin model solutions and the local complex bathymetry, could be disastrous for the dynamics of current intrusions onto the continental shelf.

At the scale of the continental shelf of the Gulf of Lion, the oceanic circulation is dominated by local winds. Because of the particular orography of the South of France, these winds are channelled. Estournel et al. (2003) showed that the wind stress curl, associated with Tramontane and Mistral, could explain the meso-scale eddy currents developing over the whole shelf. The possible suddenness and strength of these winds are likely to cause strong inertial oscillations of the current (Petrenko et al., 2005) and coastal upwelling, preferentially developing along rectilinear sections of the coast (Johns et al., 1992). In winter, these winds, rather dry and cold, extract a large amount of heat from the water column. The more the water column is shallow, the more the cooling is pronounced. Dufau-Julliand et al. (2004) showed that the dense water lenses, formed through that process on the Gulf of Lion shelf, sink along the bottom slope and that the western canyons were the principal pathway between the continental shelf and the deep sea area. The formation of dense waters over the shelf is nevertheless limited by buoyancy effects as fresh waters are brought by local rivers. Because of its strong freshwater discharge (actually the largest river discharge of the whole Mediterranean Sea), the Rhone river is an important source of potential energy that significantly influences the shelf circulation features of the Gulf of Lion. Because of the atidal context, the Rhone plume is slowly diluted with oceanic waters. The surface lenses, formed in the river mouth area, are only a few meter thick and their response to local wind variations is rather quick. Estournel et al. (1997, 2001), Marsaleix et al. (1998) and Reffray et al. (2004) studied the dynamic of the Rhone river plume, showing that the Symphonie physical model could reproduce the sharp vertical stratification as well as the quick displacements of frontal horizontal patterns.

At small scales and close to the coast, namely the Gulf of Fos (Ulses et al., 2005) the bay of Banyuls (Guizien et al., 2006) and the Gulf of Aygues Mortes (Leredde et al., 2007), the principal characteristics of the circulation have been well reproduced by the Symphonie model.

Thanks to the numerous in situ and satellite observations, all the previously mentioned studies have brought different kinds of validations.

<sup>1</sup>A weekly forecasting bulletin is provided for the north-western Mediterranean region. These bulletins are available at [www.noveltis.fr/mfstep-wp9](http://www.noveltis.fr/mfstep-wp9).

## 2.2 Description of the model

A short description of the SYMPHONIE physical model is now given. The reader can refer to the previously mentioned papers for complementary information.

The components of the current, the temperature and the salinity are computed on a staggered C-grid thanks to a classic finite difference method detailed in Marsaleix et al. (2008). The model is “free surface”, in such a way that high frequencies barotropic processes are explicitly represented. Solving surface waves is known to potentially increase computing costs. We limit this drawback by computing the baroclinic and barotropic velocity components separately, based on well adapted separated time steps, according to the time-splitting method proposed by Blumberg and Mellor (1987). Vertical turbulent fluxes are parameterized thanks to the turbulence closure scheme, based on one prognostic equation for the turbulence kinetic energy and on two length scales (for mixing and dissipation) proposed by Gaspar et al. (1990). Small scale horizontal processes, unresolved by model equations because of limitations due to the grid length scale, are parameterized through a Laplacian-type mixing operator. The horizontal mixing coefficient remains constant, as far as currents are concerned. Practically, it is equal to  $15 \text{ m}^2 \text{ s}^{-1}$  in the case of the regional model. An adaptative horizontal diffusivity is used for tracer equations in order to limit the overshoot effects of the second order centered advection scheme.

The bathymetry of the regional model of the NWM (this model is detailed in Sect. 2.4) was built thanks to two databases. The high resolution regular ( $200 \text{ m} \times 200 \text{ m}$ ) database provided by IFREMER, covering the Gulf of Lion was extended by the GEBCO one-minute data set. Thus, the computed bathymetry is essentially an average value of the database grid nodes covered by the considered model grid box. The  $2\Delta x$  signal of the bathymetry was removed thanks to a Laplacian type filter in order to avoid the growth of small numerical modes in the simulations. The filter has obviously a possible impact on larger length scales but, owing to the high spatial resolution of our grid, the slope of the continental shelf break is still faithfully represented.

As in most coastal models, a sigma coordinate type system was chosen. Indeed the sigma system likely leads to a better representation of the bathymetry than the  $z$  coordinate system, provided that some numerical contingencies (detailed after) do not impose an excessive smoothing of the model bathymetry. As far as the NWM is concerned, the bathymetry is a critical issue insofar as the Northern current is largely guided by the continental slope. The sigma-coordinate also enables to maintain a fine vertical resolution near the bottom, a significant asset since the bottom turbulence layer is likely to play a major role in the equilibrium of continental shelf circulations (Dufau-Julliand et al., 2004).

On the other hand, the sigma coordinate is known to present some serious shortcomings. Among them, the ac-

curacy of the pressure gradient is probably the most well known with the so called truncation error problem related to the sigma levels slope. Another shortcoming of the sigma system concerns the possible lack of vertical resolution in deep sea areas, or alternatively, an excessive number of vertical levels in shallow areas consequently leading to a drastic reduction of the time step in order to ensure numerical stability.

Many authors have proposed compromises to reduce those drawbacks. A common way to improve the accuracy of the pressure gradient force is to smooth the model bathymetry. Leitão et al. (2005) used a Cartesian system combined to a bottom-following first level (the so-called partial step coordinate), and Auclair et al. (2000a) proposed a two-fold sigma coordinate in order to keep the upper levels close to the Cartesian system. Another compromise is to use a generalised topography following coordinate system (Pietrzak et al., 2002). Such coordinates provide some degrees of freedom in the definition of the position of vertical levels, providing for instance a way to optimize the vertical distribution within surface or bottom layers. However, this system does not allow to efficiently control the slope of the deeper levels and to eventually avoid, for some of them, the situation of hydrostatic inconsistency (Haney, 1991), unfavourable to pressure gradient computation. We propose here to combine a generalized topography following coordinate system with a “staircases” system. This “hybrid” coordinate system (hereafter referred as to “s-step” coordinate) consists in skipping over a vertical level, as the classic Cartesian system does, when the bathymetry is too steep for the sigma level to follow the bottom slope without creating a situation of hydrostatic inconsistency. Thus, the s-step system offers the advantage of improving the pressure gradient force accuracy without employing the classical technique of smoothing the bathymetry. Another advantage is also to limit the number of vertical levels in very shallow areas, as for instance in the Rhone river mouth area, where the bottom depth reaches approximately 2 m. In our model, the Rhone estuary is partly modelled through a waterway, a few grid points long. Currents are locally very strong and a classic sigma coordinate system, including the complete set of vertical levels (40 levels in the present case), would severely restrict the time step for CFL stability reasons, among which appears the need for advection schemes to deal with current numbers lower than 1. Our s-step system uses only 5 levels in the Rhone river waterway. The principal equations of the model, formulated within the sigma coordinate system, are presented in Appendix A.

## 2.3 Open boundary conditions

### River runoff

The specification of the river run-off forcing is a key step of any modeling effort of the NWM. Indeed, this region includes the Rhone river mouth, which, with a  $1700 \text{ m}^3/\text{s}$

annual mean discharge is the largest in the Mediterranean basin. It has in particular a crucial impact on the dynamics of the Gulf of Lion. As shown in Estournel et al. (2001), the boundary condition is specified at the river mouth for the normal component of the horizontal velocity, and for both temperature and salinity at the upstream neighboring point. A vanishing salinity is imposed while a climatological annual variation is specified for temperature. A logarithmic profile is imposed for the current associated with a mass conservation criterion to insure that the river runoff is correctly specified:

$$L \int_{-h}^{\eta} u dz = F$$

where  $L$  is the river mouth width (in the NWM, the river boundary condition is specified over only one grid point, so that  $L = \Delta x$ ) and  $F$  is the observed river discharge in  $\text{m}^3 \text{s}^{-1}$ . In hindcast mode, the daily discharges for both the Rhone and Ebro Rivers are taken from CNR<sup>2</sup> and SAIH Ebro<sup>3</sup>. In forecast mode, river discharges remain constant and are taken equal to the last available observation.

### Surface conditions

Surface boundary conditions for diffusion terms in temperature, salinity, and horizontal momentum equations are respectively given by heat ( $Q$ ), salt ( $S$ ) and momentum ( $\tau$ ) surface fluxes following:

$$K_v \frac{\partial T}{\partial z} = Q (\rho C_p)^{-1}, \quad K_v \frac{\partial S}{\partial z} = F \rho^{-1} S, \quad K_v \left( \frac{\partial u}{\partial z}, \frac{\partial v}{\partial z} \right) = (\tau_u, \tau_v) \rho^{-1} \quad (1)$$

where  $C_p$  is the ocean heat capacity ( $3950 \text{ J/kg/K}$ ). The heat flux includes the net long wave radiation ( $Q_L$ ), sensible ( $Q_H$ ) and latent ( $Q_E$ ) heat fluxes. The salt flux is made of precipitation ( $P$ ) and evaporation ( $E$ ) fluxes. This latest component is directly related to the latent heat flux ( $Q_E \approx 2.5 \times 10^6 E$ ).

The turbulent heat and momentum fluxes are estimated from classical meteorological variables through bulk formulae (Geernaert, 1990) detailed in Appendix B.

Practically, hourly values of the wind at 10 m high, of the surface pressure, of the specific humidity, of the air temperature at 2 m high, of the precipitation, of the solar radiation and of the longwave radiation received by the ocean from the atmosphere ( $Q_A$ ) are provided by the meteorological model ALADIN (Brožková et al., 2006). The net longwave flux is deduced from  $Q_A$  thanks to the sea surface temperature and the Stefan constant ( $\sigma = 5.67 \times 10^{-8} \text{ W m}^{-2} \text{ K}^{-4}$ ):

$$Q_L = Q_A - \sigma T_{0m}^4 \quad (2)$$

<sup>2</sup>CNR: <http://www.cnr.tm.fr>

<sup>3</sup>SAIH Ebro: <http://195.55.247.237/saihebro/>

### Lateral open boundary conditions

Open boundary conditions (OBC) are discussed in detail in Marsaleix et al. (2006) and are thus briefly presented here. Classically, OBC endorse here a double purpose: they are first of all required to force the inner solution with the external fields obtained from the large-extent model and at the same time, they must allow waves to radiate out or water masses to leave the modeling domain under outgoing conditions, without any spurious reflections. The Flather scheme gives a boundary condition for the sea surface elevation. A zero gradient condition is applied to the tangential component of the transport while its normal component is deduced from the two former variables combined to the inversion of the barotropic continuity equation. Marsaleix et al. (2006) showed that such an implementation of the Flather conditions offers interesting properties of mass and energy conservation. A wave-equation-type condition, or Sommerfeld condition, based on a constant wave speed of 1 m/s, is applied to the baroclinic horizontal velocities. The tracer condition is simply given by the inner advection diffusion equation (Appendix A, Eqs. A4 and A5) but with an upstream version of the advection scheme in order to make the external water masses enter the numerical domain under inflow conditions. OBC are combined with a restoring condition toward the external field within a nudging layer, in the vicinity of open boundaries. Within this layer the restoring term is added to the momentum and tracer equations. This term, which is progressively vanishing with the distance to the open boundary (practically the layer is 15 grid points wide), is inversely proportional to a time scale equal to one day (for baroclinic velocities and tracer equations) and to 0.05 day (for barotropic velocities equations) at the closest grid nodes to the boundary.

### 2.4 Operational forecasting system for embedded modeling

The regional modeling of the NWM is based on a  $3 \text{ km} \times 3 \text{ km}$  grid (Fig. 1). The hybrid vertical sigma grid has a maximum of 40 levels above the abyssal region, 20 levels over the shelf and only 5 levels in the shallower regions, such the Rhone river mouth. A rotation of the model grid with respect to the North-South direction is made in order to optimize the modeling of the cyclonic regional circulation made of the Northern Current along the Northern coastline (Millot, 1990).

The regional model is initialized and forced at its boundaries by the general circulation model (GCM) OPA implemented at the  $1/16^\circ$  horizontal resolution (Tonani et al., 2008). At forecasting scales, i.e. a few days, the model “spin up” remains a challenging problem. Indeed, “spin up” has classically been considered as a troublesome but “self-resolving” difficulty. If long, tedious spin up periods could be carried out in process oriented studies, it cannot be tolerated

in realistic “scale oriented” modeling whether operational or not (Auclair et al., 2006).

Over the shelf break and in the coastal region, the bathymetry mismatches between the low and high resolution models necessarily break the fundamental physical balances (Auclair et al., 2000b or 2006). A two step strategy is thus proposed for the NWM embedded modeling.

### VIFOP optimization

Optimal extrapolation and mass balance enforcement are carried out before larger scale fields are used to initialize and force the embedded, high resolution model along its open boundaries. This is obtained thanks to the Variational Initialization and Forcing Platform (VIFOP). The objective of this variational optimization strategy is first to ensure that the forcing fields satisfy the fundamental mass balance. As a consequence, no spurious mass exchange can appear associated for instance to a crude interpolation scheme over regions showing large bathymetry mismatches. The second objective is to drastically reduce the generation of surface gravity waves due to a local mass unbalance. Such waves have been shown to last for a few hours to several days following the initialization (Auclair et al., 2000b). The optimal extrapolation is used to initialize regions where no information is available (Auclair et al., 2006). Such regions can in particular be found along the shelf break where the GCM bathymetry can be several tenths of meters shallower than the high resolution embedded model. In these areas, crude interpolation most often lead to the generation of spurious geostrophic currents which can hardly be separated from physically coherent along-shelf currents (Auclair et al., 2006).

### Small scale spin-up

On the other hand, small scale turbulence together with small scale ocean dynamics associated for instance to atmospheric forcing cannot be a priori adjusted at the initial time step and usually take a few days to build up and adjust. Indeed, regional models are basically used to downscale the GCM large scale dynamics in which XBT and satellite observations have both been assimilated. They are thus based on a high quality large scale dynamics and, thanks to their higher resolution, they additionally provide smaller scale dynamics. In the frame of the MFS, five-day forecasts are issued and small scale dynamics must have grown up to their realistic level at the beginning of the forecast. The regional modeling must thus begin a few days before the forecast period.

### The pre-modeling/forecast strategy

If a few-day “pre-modeling” has thus to be systematically carried out before the forecast period, this period must remain as short as possible for at least two reasons. On the one hand, coastal ocean predictability is not infinite and on the other hand, the CPU time must remain affordable.

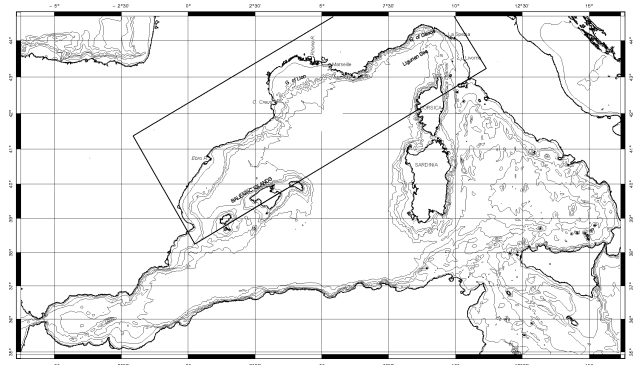


**Fig. 1.** Implementation of the Northwestern Mediterranean regional model.

As a compromise, a one-week period is chosen for pre-modeling. The GCM delivers each week analyses for the previous fifteen days and ten days of forecast (Tonani et al., 2007). The meteorological ALADIN model delivers analyses for the previous seven days and a 5-day forecast.

As soon as these products are available on ftp sites, the regional forecast can start (Fig. 2). First the pre-modeling corresponding to the hindcast of the previous seven days is done using analyzed atmospheric fluxes, GCM analysis as initial condition and forcing along its open boundaries and, when available, in-situ observations for river discharges. Then, the same numerical run is pursued during 5 days in forecasting mode, based on forcing by atmospheric and GCM forecasts. This 12-day modeling procedure is repeated every week.

In order to clearly evaluate the quality of such forecasts during the 6-month “TOP” of the MFSTEP, a similar regional modeling was conducted in which only analyses were used for atmospheric, oceanic and river forcing. This “hindcast” modeling identical to the forecast modeling during the first seven days of pre-modeling has been used as a reference to evaluate the quality of the five-day forecasts.

## 3 Evaluation of the forecasting system

### 3.1 Diagnostics on embedded forecast

A set of six forecast periods has been selected and is now analyzed in detail. Three of them are chosen at the end of the summer period (September–October), i.e. for stratified conditions in the upper ocean, while the remaining three forecast periods are chosen in winter, i.e. for well mixed conditions.

#### Pre-modeling period

Figure 3 shows the time evolution of the current intensity averaged over the 6 selected forecast periods and over the domain. In order to clearly extract the spin up of the small scale structures, the current has been decomposed as  $V = \bar{V} + V'$

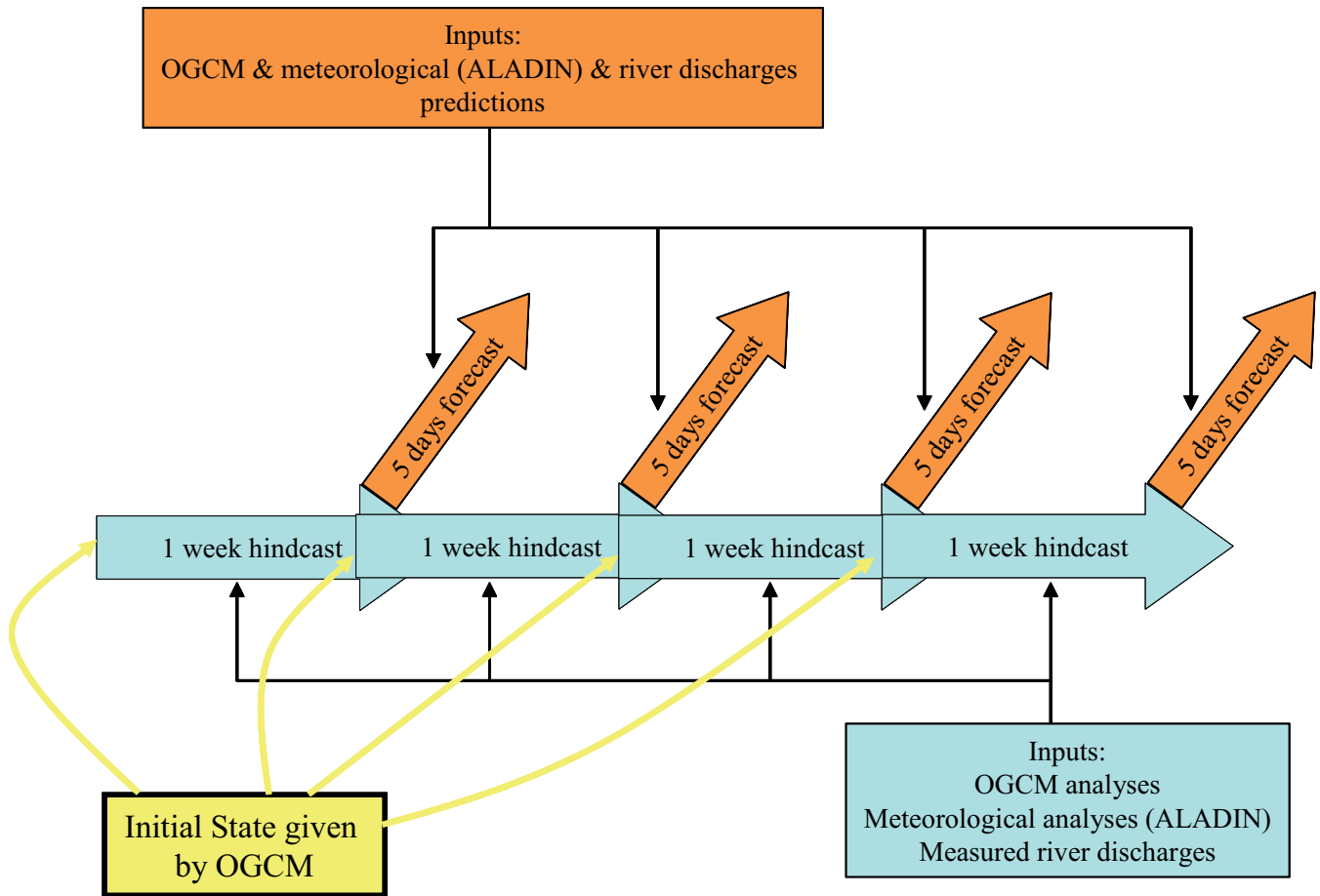


**Fig. 2.** Scheme of the operational sequence of the regional NWM model.

where  $\bar{V}$  is the large scale component and  $V'$  is the small scale anomaly. The large scale component of the current is computed as the windowed averaged current over a 33 km square box around each grid point. To be compared, both regional and GCM fields have been averaged over a 24-h period.

We can globally notice that the obtained large scale currents are rather similar and show in particular the same temporal variations. Figure 4 presenting the large scale currents at 100 m on 18 January 2005 at the end of a hindcast period shows that spatial structures are also the same at large scale.

At smaller scales, the GCM currents are, as could be expected, rather small while the regional model, thanks to its higher resolution, progressively grows a small scale dynamics starting at the initialization date. It can be noticed that the growth of these smaller scales is rather steep during the pre-modeling period but slows down during the 5-day forecasting period. The length of the 7-day pre-modeling period appears thus to be justified with regard to the small scale growth rate in the regional model.

### Comparison of the regional and GCM dynamics

Based on Fig. 3, it has thus been shown that large scale currents are globally similar in the regional model and in the GCM. In order to give finer criteria for their comparison, the time evolution of both the regional model biases (see Eq. 3) and of the rms errors (see Eq. 4) relative to the GCM has been computed at different levels  $z$  along the 12 days of simulation (pre-modeling and forecast) and is shown in Fig. 5.

$$\text{bias}(\text{reg.}, \text{GCM}, \phi, z) = \frac{\sum_{i=1, N} (\phi_i^{\text{reg}}(z) - \phi_i^{\text{gcm}}(z))}{N} \quad (3)$$

$$\text{rms}(\text{reg.}, \text{GCM}, \phi, z) = \sqrt{\frac{\sum_{i=1, N} (\phi_i^{\text{reg}}(z) - \phi_i^{\text{gcm}}(z))^2}{N}} \quad (4)$$

where  $\phi$  is the selected variable (temperature, salinity, current) and  $N$  is the number of grid points at the depth  $z$  considered. For the GCM, we use the fields interpolated on the regional grid by VIFOP.

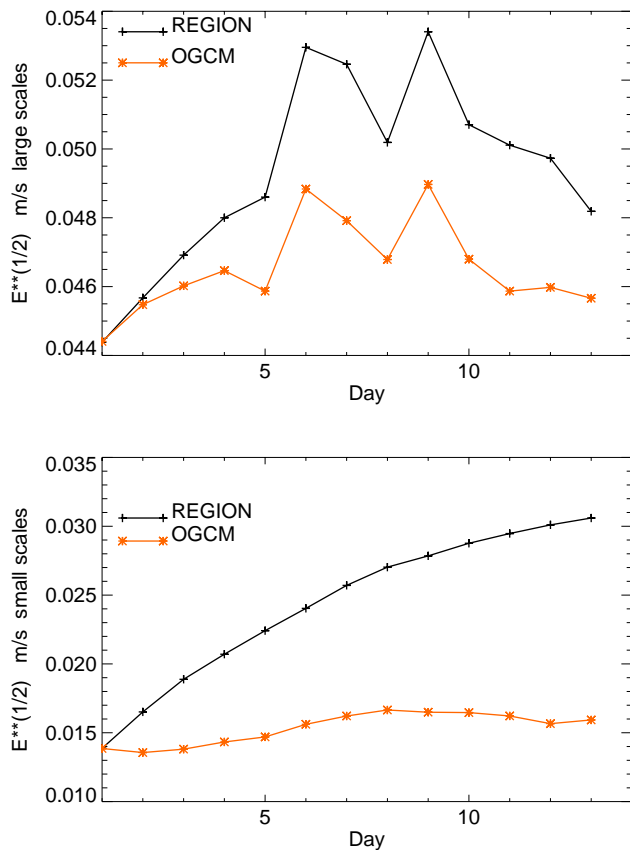


**Fig. 3.** Mean evolution of the spatially averaged kinetic energy root mean square during the twelve days of simulation. Kinetic energy has been splitted in a large scale component and small scale component. Results are presented for the regional model and for the GCM.

The biases are thus globally small with respect to rms errors and decrease with depth. They have an opposite sign at depth of 1 m and 30 m. This leads to the conclusion that vertical gradients are smoother in the regional model than in the GCM. This is most likely due to a stronger level of turbulence in the regional model in the upper layer.

Biases in global mean measures being relatively small (in particular for salinity), a large part of the rms errors can be thought to be a result of small scale dynamics or of differences between meteorological forcing in regional and general circulation models. A comparison has been made between the wind stress calculated on one hand by the regional model using the Aladin model at the horizontal resolution of  $0.1^\circ$  and on the other hand by the GCM using the ECMWF forcing at about  $0.5^\circ$ . A period of 9 days (11–19 November 2004) characterized by strong wind blowing offshore has been chosen (Fig. 6). Although maximal values and general patterns are similar for both fields, some differences appear that can be related to the representation of orography. Compared to ECMWF, the Aladin model produces lo-

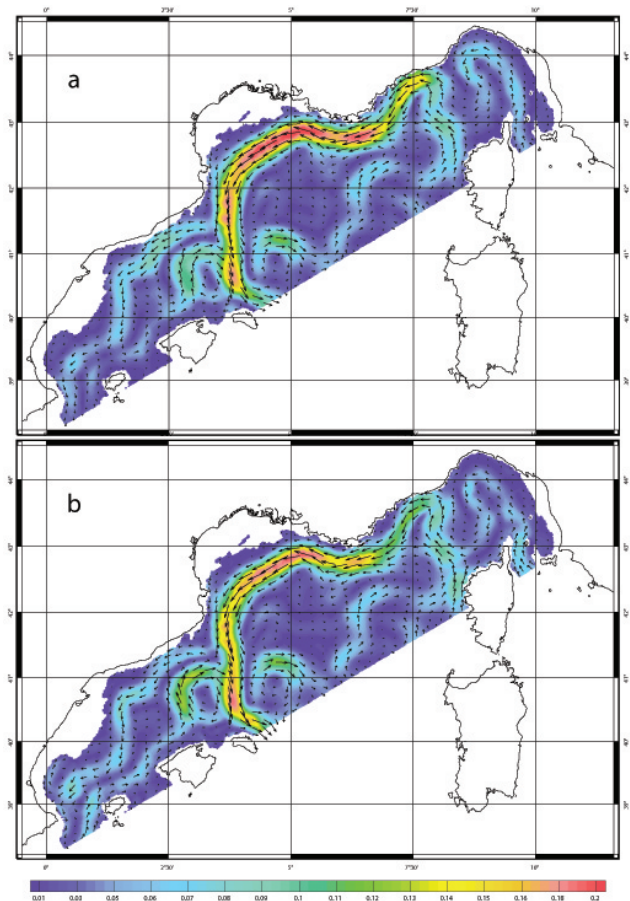


**Fig. 4.** Large scale component of the current at 100 m modelled by (a) the NWM regional model, (b) the GCM (interpolated on the regional model grid).

cal winds which are more channelled in the valleys (see the Ebro valley in Spain, the region of Genoa or the Arno valley) while the reduction of the flow is also more important downstream of mountains. Large differences can be noticed on the west coast of the Gulf of Lion where the Tramontana wind from Aladin blocked by the Pyrenees blows eastward inland and then turns southward at the extremity of the Pyrenees as observed during the PYREX experiment (Georgelin and Richard, 1996) while this diversion of the flow is not so clear from the ECMWF forcing. These orographic effects result in enhanced wind curls which are able to generate temporary eddies on the shelf (Estournel et al., 2003) or vertical velocities offshore. Besides the analysis of the regional model behaviour based on spatial averages, it is interesting to consider the localization of the differences between the regional model and the GCM. A typical example is presented on Fig. 7 showing the 30 m deep current calculated by both models on 17 November 2004 during the strong wind period of Fig. 6. The main tendency for the open sea is that the regional model currents are often narrower and slightly stronger than those

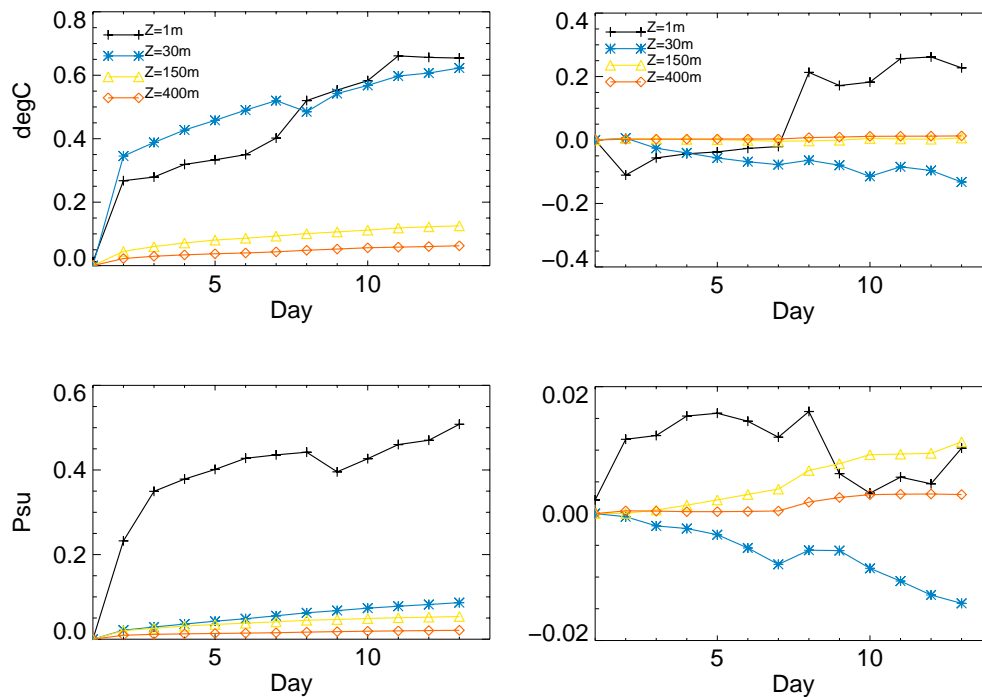


**Fig. 5.** Bias (right panel) and rms error (left panel) of the regional model (see Eqs. 3 and 4) with respect to GCM calculated for temperature (upper panel) and salinity (lower panel) at different levels.

of the GCM. Important differences appear on the shelf: first an intrusion of the Northern current on the shelf at the eastern entrance of the Gulf of Lion (around  $5^{\circ}20'$  E). This mechanism was observed in a large number of situations (Gatti, 2008). The resolution of the model is probably crucial to capture this process. The second point is the circulation in the western part of the Gulf of Lion which is anticyclonic in the GCM (northward current along the coast) and opposite in the regional model (southward current fed by a strong intrusion of the Northern current around  $4^{\circ}$  E). These differences are related to the wind fields used by both models (Fig. 6). In the GCM (Fig. 6b), the wind maximum is not stuck to the west coast resulting in a negative wind curl southwest of this wind channel creating the anticyclonic circulation. In the regional model, the wind field (Fig. 6a) is dominated by a positive wind curl northeast of the wind maximum inducing the cyclonic circulation.

Close to the surface, large discrepancies can be observed over the salinity fields due to the differences in the river fresh water forcing strategies in both models. If explicitly forced in the regional model, such forcing is indeed applied through the relaxation of surface salinity in the GCM. Temperature, which is less affected than salinity by river discharges due to the temperature contrast between river and sea lower than the salinity contrast, only shows a steep increase of its rms errors during the very first day. After this period of adjustment, the rms increase remains regular and smoother during the remaining of the modeling period.

### 3.2 Predictability at regional scale

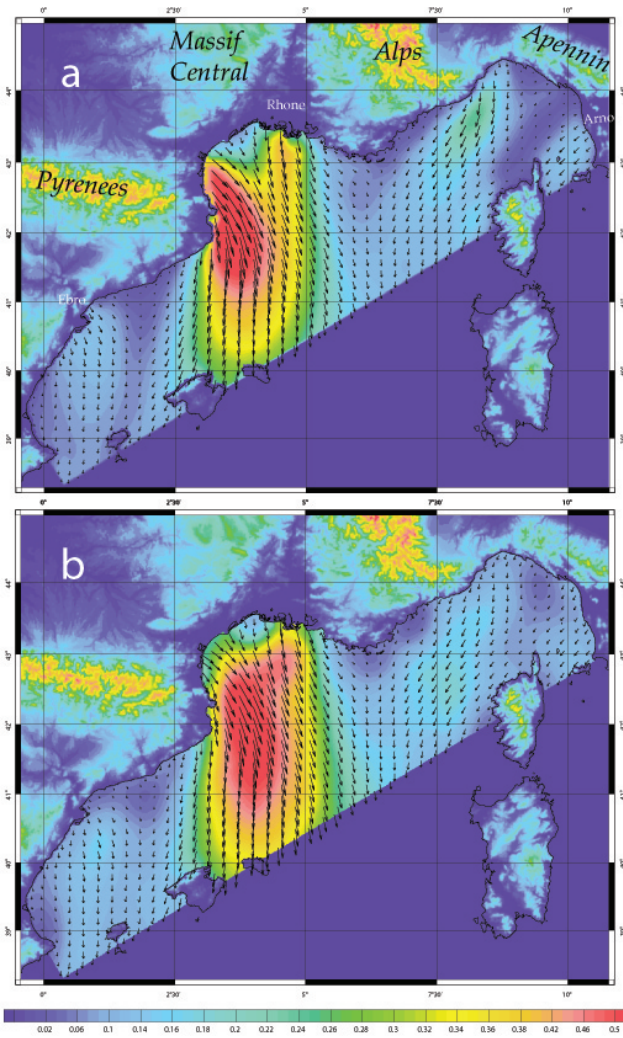
In order to study the effectiveness of the forecast strategy, the forecasted fields are now compared to the hindcast reference fields. The rms errors have been computed for temperature, salinity and currents for the whole modeling period at 4 different depths over the complete domain. Figure 8 shows that rms errors remain rather small at depth. Far from the surface, these differences can most likely be attributed to the differences between the forcing fields used both to initialize and force the regional model along its open boundaries: in one case the GCM forecasts are used while in the other case only analyses are considered. In the upper part of the ocean, differences in meteorological analysis – forecast forcing are mainly responsible for such mismatches which remain at a very low level probably because of the strong wind conditions which prevailed during the period.

### 3.3 Comparison to the observing system

The forecast issued during the 6 selected periods are now compared to satellite SST observations and to in situ MedArgo observations. A statistical analysis is given.

#### SST observations

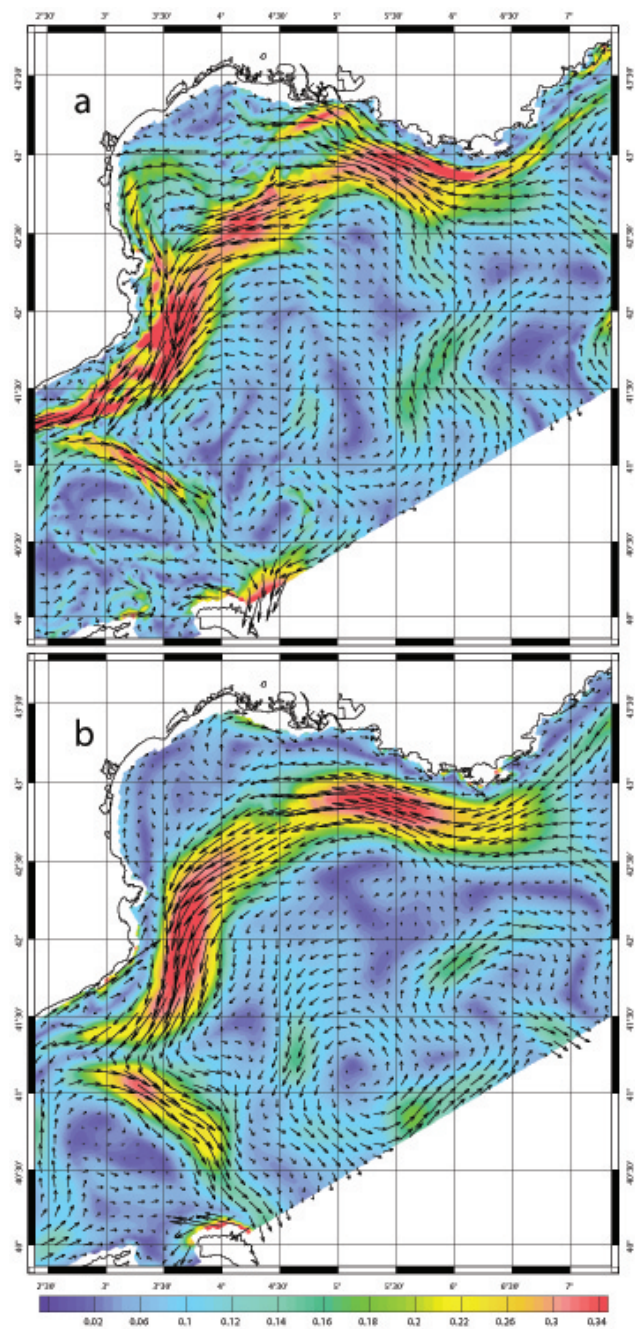
The temperature at the regional model first level under the surface is compared to cloud free, AVHRR Oceans Pathfinder SST pictures which have been interpolated over



**Fig. 6.** Wind stress averaged over the 11–19 November 2004 period, produced by (a) the NWM regional model forced by Aladin, (b) the GCM forced by ECMWF (interpolation on the regional model grid). The continental orography has been superimposed to interpret the wind stress field.

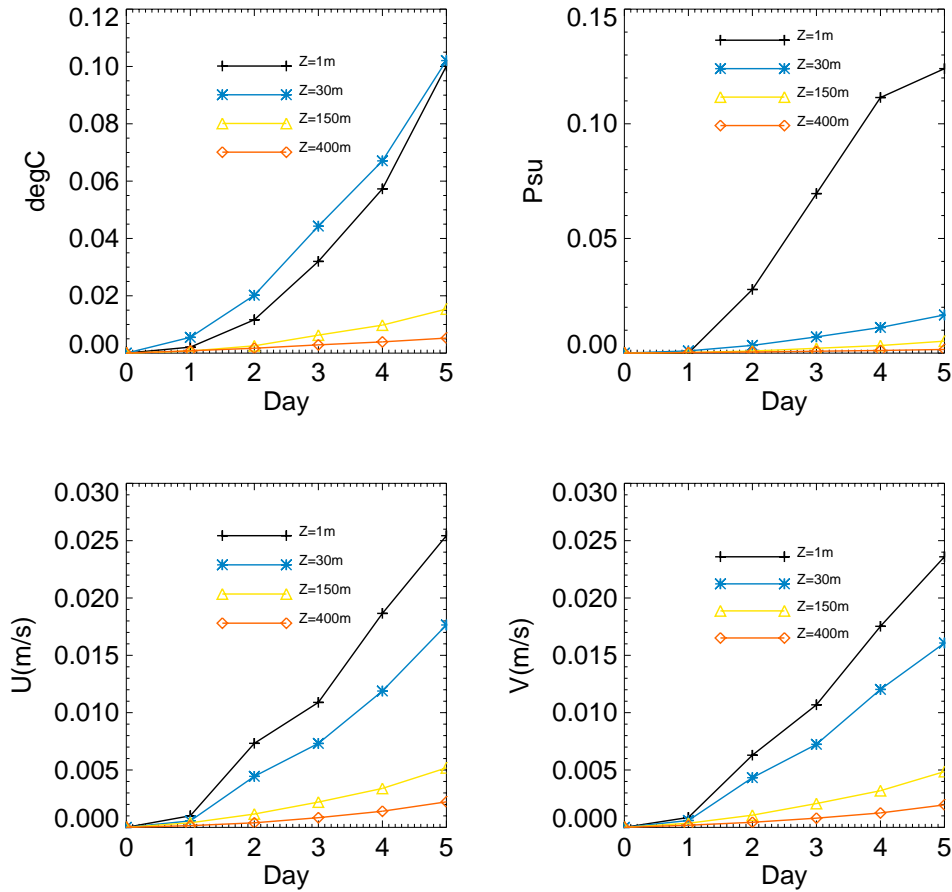
the 1/16th of degree GCM grid (Marullo et al., 2007). The 13-day averaged biases and the rms errors have been computed for each modeling period in order to evaluate the seasonal evolution of the errors (Fig. 9a). Then biases and rms errors have been additionally averaged over the selected forecasts in order to evaluate their evolution over a typical forecasting period (Fig. 9b).

Figure 9 clearly shows that 60 to 65% of the discrepancies between forecasts and observations correspond to a negative bias. Rms errors grow up during the first 2 to 3 days following the initialization before stabilizing. This can be due to an adjustment of the regional model initial conditions through vertical mixing. Initial conditions are provided by the GCM which uses a turbulence scheme and meteorolog-



**Fig. 7.** Current at 30 m on 17 November 2004 modelled by (a) the NWM regional model, (b) the GCM (interpolation on the regional model grid).

ical forcing fields different from those used by the regional model, the former in addition assimilating SST. The regional model reacts to this initial condition by increasing the initial bias during the first days up to a stationary value. As could be expected, error levels are larger during the “stratified” periods than during the winter periods which correspond to well-mixed regimes. Indeed, in these latter cases,



**Fig. 8.** Evolution of the rms error of the forecast with respect to the hindcast calculated for temperature, salinity and the two components of the current at different levels.

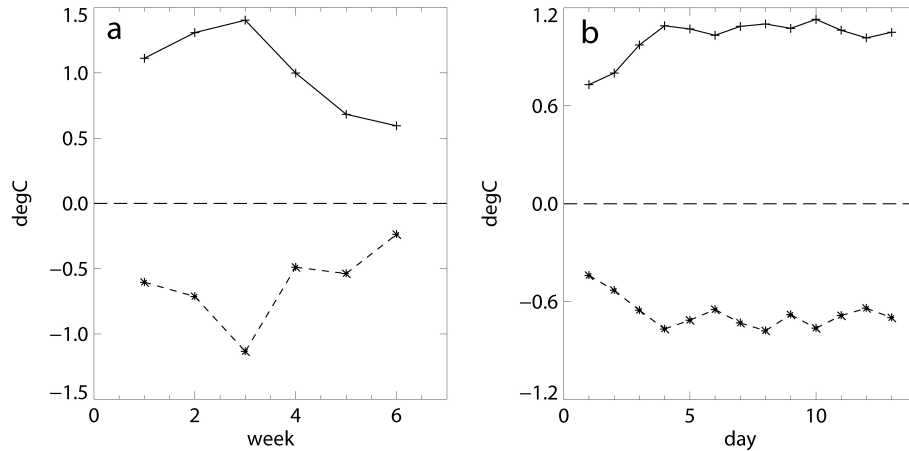


**Fig. 9.** rms error (solid line) and bias (dashed line) of the regional model with respect to satellite SST. (a) Each point corresponds to an average over a 13-day forecasting period; (b) Each point corresponds to a daily average of the six selected forecast periods.

the influence of the turbulent scheme is much smaller. In the following paragraph, further comparisons with temperature observations based on vertical profiles will bring more information on this bias.

### Med-Argo observations

When and where they are available, MedArgo temperature and salinity profiles give complementary and fruitful

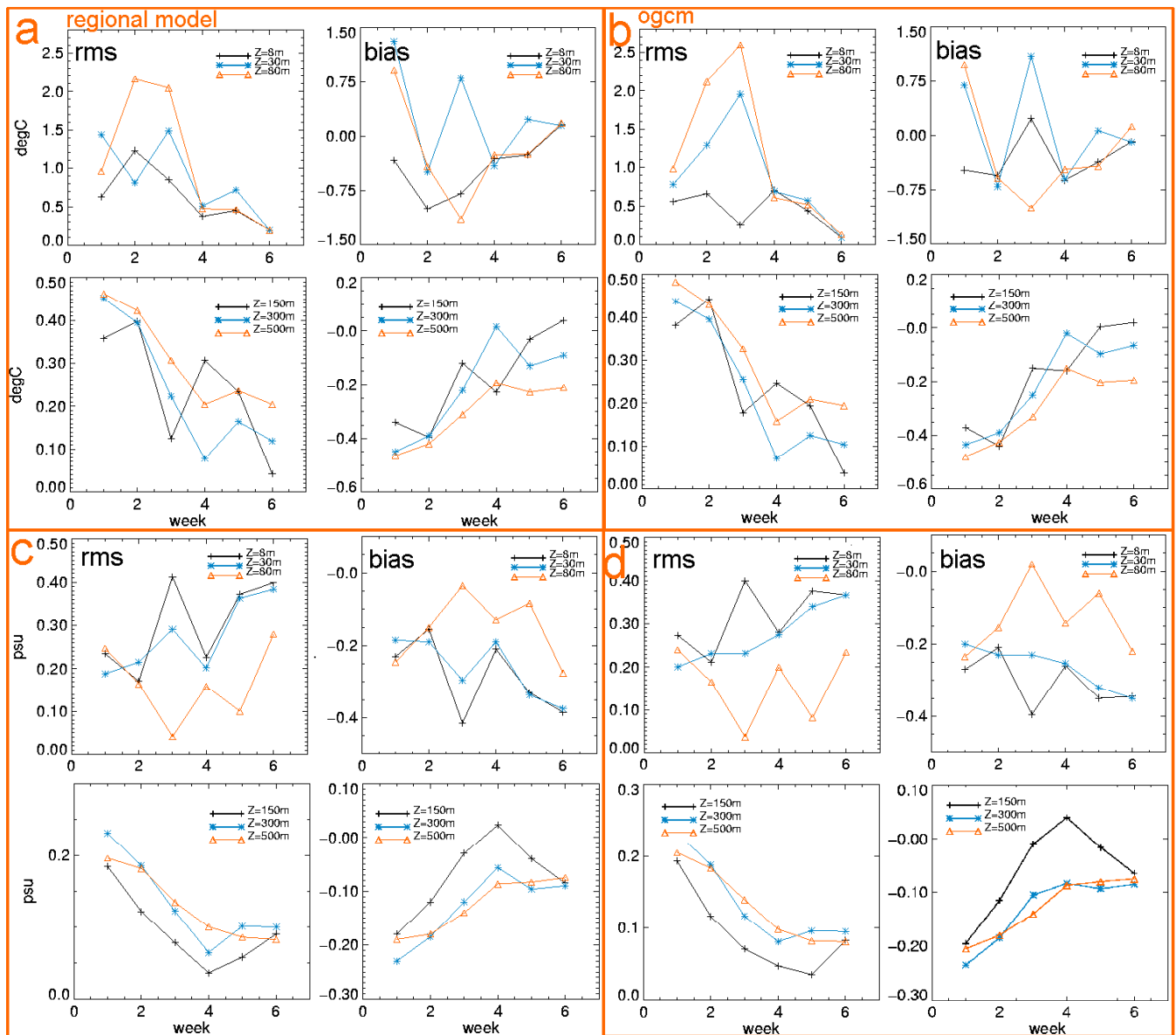


**Fig. 10.** (a) and (c) rms error and bias of the regional model with respect to MedArgo temperature and salinity observations. (b) and (d) rms error and bias of the MFSTEP GCM with respect to MedArgo temperature and salinity observations on the domain of the NWM model.

information and are assimilated by the GCM. They in particular offer a unique opportunity to compute both temperature and salinity biases and rms errors at depth. About 60 vertical profiles have been made by the four MedArgo profilers in the NWM region for the 6-month period (Emelianov et al., 2006). A first group of profiles is located close to the Corsica western coast while the remaining is spread in the Balearic Sea. To perform a comparison, the forecasted temperature profile at the closest grid point is selected at the observation dates. Figure 10a shows for the selected periods, temperature biases and rms errors at 6 depths (8 m, 30 m, 80 m, 150 m, 300 m and 500 m) for the regional model and for the GCM.

At 8 m deep, temperature MedArgo observations lead to the same conclusion as SST satellite observations, i.e. the presence of a negative bias which is larger in fall than in winter. Even if only a few profiles are available, the differences between forecast and observations have the same order of magnitude as for SST observations. At 30 m deep, results are rather different as, when significant, the bias is positive. At 80 m deep, the differences between the regional model and the observations are rather large but are not associated with any biases. The errors of the GCM are close to those of the regional model, the largest difference between the two models concerning temperature at 8 m which is more accurately represented by the GCM.

It can thus be concluded that the underestimation of temperature by the regional model just below the surface and its overestimation at 30 m deep can be attributed to an overestimation of the turbulent mixing. SST assimilation is expected to be responsible of the better performance of the GCM for representing temperature near the surface especially because both models provide very close scores for 8 m salinity. At 80 m deep, the differences could be attributed to a localized wrong representation of the water masses in fall. A similar comparison of the forecasted temperature profiles with XBT and CTD profiles (not shown) has also been carried out. It shows very similar results above 30 m, whereas at 80 m deep, the differences are much smaller than for the MedArgo observations. This would be coherent with a localized underestimation of temperature at 80 m evidenced by the MedArgo profilers.

Deeper, at 150, 300 and 500 m, Fig. 10a shows similar errors corresponding mainly to negative biases of the regional model. These errors are very close to the GCM ones (Fig. 10b) and are thus a direct consequence of the initialization. Surprisingly enough, this bias decreases during the forecast period. An explanation could be that the MedArgo observations are assimilated by the GCM and as a consequence are not independent observations. The characteristics of the different water masses and in particular of the Levantine Intermediate Waters (LIW) can thus be recovered in the GCM. Another more physical explanation could be attributed to the seasonal evolution of the LIW main characteristics in the Eastern Mediterranean basin where they are formed or alternatively to mixing with other water masses by winter convection in the NWM basin. This study should be continued for at least one complete annual cycle to better understand the evolution of the quality of the simulations.

An analysis of the salinity errors (Fig. 10c) shows negative biases at nearly all levels. Unlike what was found for temperature, this bias does not change sign in the surface layer. It remains very close to the GCM biases (Fig. 10d). This is due to the fact that, unlike temperature, salinity does not change significantly during this short term forecast and consequently remains close to the initialization field. At depth, the salinity bias decreases with time: this was previously found for temperature.

In the surface layer, the high resolution meteorological forcing, the turbulence flux parameterization and the fresh water forcing are in large part responsible for the quality of temperature and salinity vertical gradients. At depth, when the regional model is embedded in a larger scale model and without specific assimilation, the quality of the regional scale forecast is primarily constrained by the quality of the GCM. In the NWM, the largest bias is negative affecting salinity which decreases in deeper layers but remains large in the first 100 m, leading thus to too light subsurface waters. This analysis has principally been achieved in the central region of the basin where the majority of the vertical profiles have been measured but a limited number of profiles have been

additionally made directly in the Northern Current along the Spanish slope. In a further study, a distinct analysis of the bias in both water masses should provide a quantification of the errors on the horizontal density gradients and, as a consequence, on the strength and the vertical profile of the Northern Current.

#### 4 Scale oriented analysis of several processes in the NWM

Two hydrodynamic processes have been selected, each being associated with a particular range of scales of the NWM dynamics. For each process, satellite images are available and are used to validate the regional model forecast. At larger scale, the general circulation features and the dense water spreading are studied. At smaller scales, a wind induced coastal upwelling and the resulting vertical mixing in stratified conditions are then considered in detail.

##### 4.1 Main hydrologic and hydrodynamic characteristics of the Northwestern Mediterranean in winter

Observations and meteorological models show that winter 2004–2005 in the northwestern Mediterranean was characterized by periods of persistent cold and dry northerly wind. A set of deep temperature and salinity profiles sampled in the Western Mediterranean during July 2005 showed that the properties of the deep water changed abruptly with a temperature drop compensating the increase accumulated in the last ten years (Lopez-Jurado et al., 2005). These two observations suggest that strong convection took place in the MEDOC area during this winter. Both the GCM and the regional model indicate that convection broke the Levantine Intermediate Water around 42° N and 5° E at the end of January.

The satellite image of 21 January (Fig. 11a) gives information about the extent of cold waters both along the coasts and offshore. The corresponding modeling by the regional model (Fig. 11b) shows a correct localization of cold waters in the Gulf of Lion, along the Spanish coasts and along the Tuscany coasts between La Spezia and Livorno.

Offshore, cold waters are isolated from the coast by the Northern Current perceptible by its higher temperature from the Corsica channel till the western tip of the Gulf of Lion. At this point, the simulation results indicate that the current is divided into two veins: one characterized by less intense currents following the Spanish slope bounding the shelf narrow in the north and widening near the Ebro mouth while the other turns southward and follows a cyclonic pathway around the convection area. Between the Balearic Islands, the warmer and less saline Atlantic water flowing from the south of the basin penetrates northward beyond 41° N which does not look realistic compared to the satellite image.

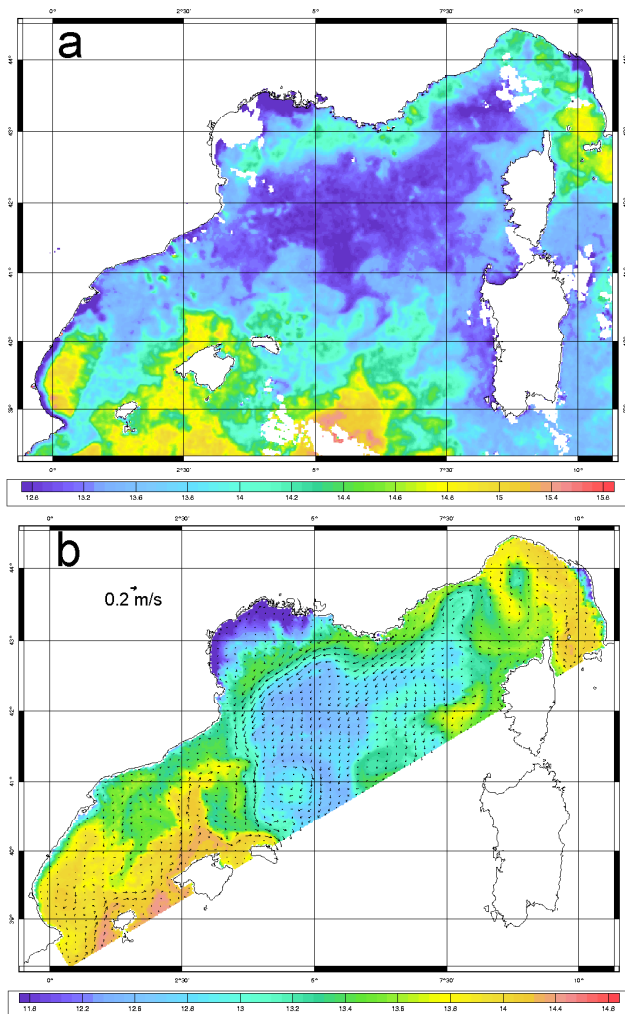


**Fig. 11.** Sea surface temperature (a) from NOAA AVHRR satellites distributed by DLR (b) from the NWM regional model corresponding to the 21 January 2005. The simulated current at 20 m under the surface has been superimposed on (b).

The simulations indicate that the weakening of the along-slope vein of the Northern Current and the corresponding strengthening of the south branch of the cyclonic circulation is likely linked to strong wind bursts in the Gulf of Lion. However observations of slope currents in the region do not seem to corroborate this process (Jordà, 2005). The underestimation by models of salinity (Sect. 3.3) and density in the subsurface waters could be responsible of erroneous circulation patterns in this region.

#### 4.2 Wind induced coastal upwelling and mixing in stratified conditions: the case of 25 September 2004

The period of 20 to 24 September is characterized by a north-westerly wind blowing over the Gulf of Lion and extending over the western Ligurian Sea (Fig. 12a). Then, starting on

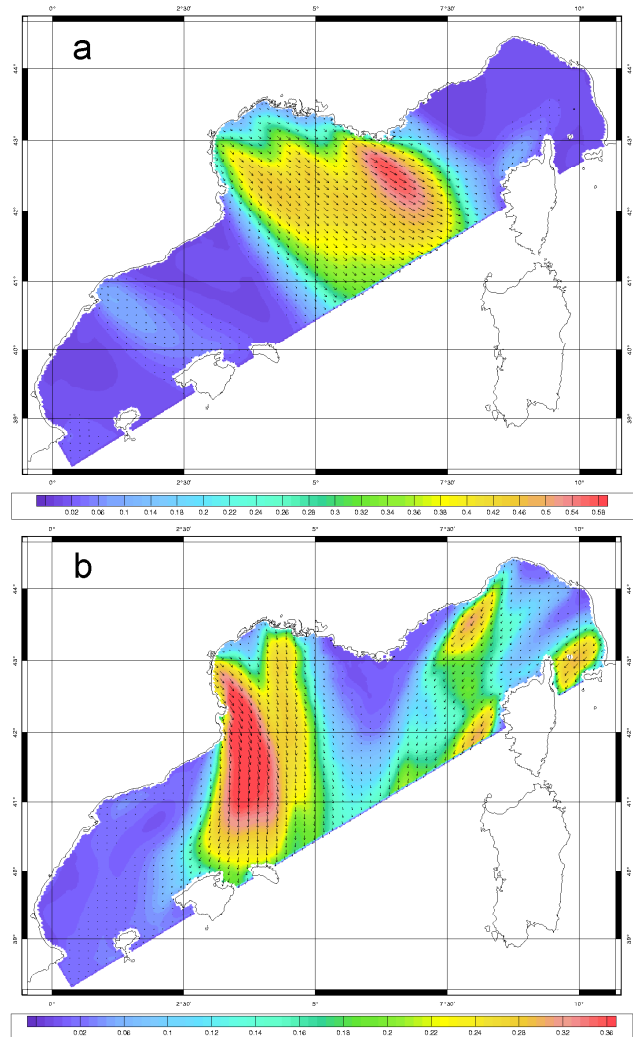


**Fig. 12.** Wind stress (N/m<sup>2</sup>) calculated from the ALADIN model wind for (a) 24 September 2004 (b) 27 September 2004.

the 25th, a classical configuration of winds settles over the region of the Gulf of Lion. It is made of the channeled Mistral and Tramontane winds (Fig. 12b). In both situations, the northern part of the Gulf of Lion is in upwelling conditions. This can clearly be seen both on the satellite picture (Fig. 13a) and on the regional forecast (Fig. 13b) where cold waters appear along the coast. The coastal region is not the only area where waters have been cooled down, as the strong wind burst has strongly cooled offshore waters.

The Gulf of Genoa and the region of the Corsica Island are isolated from the wind burst and consequently appear warmer both on satellite picture and in the regional forecast. Southwest of the Gulf of Lion, only the Ebro valley is submitted to a significant wind forcing. Over this region, this wind has yet for consequence a slight cooling of the sea surface while the surrounding waters remain warmer. Such

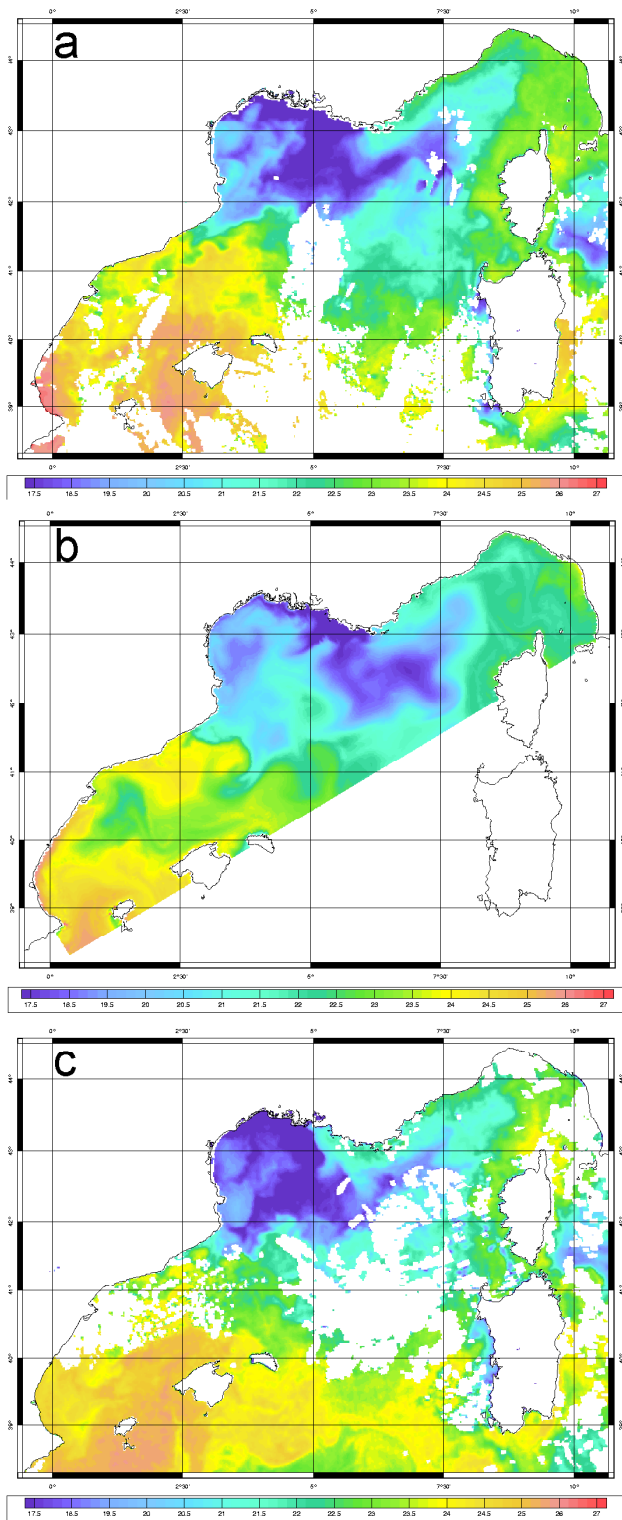


**Fig. 13.** Sea surface temperature (a) from NOAA AVHRR satellites distributed by DLR for 25 September 2004 (b) from the NWM regional model for 25 September 2004 (c) from NOAA AVHRR satellite for 28 September 2004.

warmer waters can also be found along the coast south of the Ebro mouth. The largest mismatch of the model forecast can be found north of the Majorca Island with much colder waters than in the satellite picture.

Estournel et al. (2003) have shown that, in Mistral and Tramontane conditions, a branch of the Northern current could penetrate over the western part of the shelf (around longitude  $3.5^{\circ}$  E). However, at the eastern entrance of the Gulf of Lion, the influence of the northerly winds on the Northern Current is yet poorly known. Satellite picture and model results allow to study the consequence on the current of the wind regime change occurring on 25 September. During the first wind period of Fig. 12a, the surface current characterized by relatively warm waters seems to be stopped along the Ligurian coast at about  $6^{\circ}$  E of longitude (Fig. 13a). A steep thermal front separates these waters from the colder upwelling waters which are spreading from the north-eastern coast of the Gulf of Lion. During the Mistral and Tramontane period of Fig. 12b, the eastern part of the Gulf is not submitted to strong wind conditions and a positive wind curl settles down east of the Rhone valley. On 28 September the SST satellite image (Fig. 13c) shows that the Northern current has progressed along the coast in the direction of the Rhone river mouth. Figure 14 shows a superimposition of the forecasted surface temperatures and currents for 25 and 29 September. At the eastern boundary of Fig. 14a, the Northern current separates into a coastal branch which is blocked by the upwelling colder waters and a second offshore branch. On Fig. 14b, the coastal branch of the current has progressed further and clearly penetrates over the shelf between Marseille and the Rhone river mouth.

No clear dynamical mechanism has so far been proposed to explain this process: either the decrease of the wind strength in the eastern part of the shelf or the wind curl could for instance offer local explanations for the current behavior. Otherwise, a consequence of the Tramontane wind is to push the water outside the Gulf of Lion shelf in its south-western part (Estournel et al., 2003; Ulses et al., 2006). This process could also have a remote influence on the incoming of the Northern current over the eastern part of the Gulf. The understanding and the quality of the representation by the models of these shelf/slope exchanges is crucial as it governs the renewal of the shelf waters.

## 5 Concluding remarks

In the frame of the Mediterranean Forecasting System, we have developed an embedded forecasting system in the North Western Mediterranean. This project gave us the opportunity to move from classical “process oriented studies” to more realistic “scale oriented studies” and to achieve long term forecast of the NWM in which processes are validated at each stage of the embedded modeling. In the present

configuration, dedicated observations have been assimilated in the basin scale GCM.

The regional NWM embedded forecasting system is based on the Symphonie hydrodynamic free surface model and on the variational initialization and forcing platform VIFOP. A 5-day forecast can be issued after a pre-modeling period of 7 days. This is one of the main results of the present study. Indeed, it has been shown that the development of small scale processes necessitates a one week “hindcast” (pre-modeling period) during which the forecasting capability of the embedded model is dubious. This was confirmed by a comparison of the evolution of the small scale kinetic energy in the low and high resolution models. These results are promising but we feel that progress still need to be accomplished to improve the regional forecast by taking full advantage of the complementary natures of the basin-scale forecasting system which accurately provides the larger scale structures and the water mass properties thanks to data assimilation and of the regional modeling which represent small scales created by energy cascades, by interactions with bathymetry or by mesoscale atmospheric structures thanks to fine representation of bathymetry and meteorological parameters.

The NWM system provides each week a 5-day forecast illustrated by a bulletin published on the web; these forecasts have been compared to the MFS observing system. It was basically found that in the first 100 m under the surface, the NWM model forecasts are characterized by large negative biases of salinity leading thus to too light subsurface waters. These biases are very close to the GCM ones as salinity is strongly dependent on the initial conditions for such short runs. Deeper, at 150, 300 and 500 m, the negative bias is reduced and above all, it decreases gradually as time goes on. It will be interesting to check if the assimilation of ARGO profiles in the GCM is responsible for these improvements as suggested by Tonani et al. (2007). Concerning temperature, its underestimation by the regional model just below the surface and its overestimation at 30 m deep can be attributed to an overestimation of the turbulent mixing. To go further, it would be necessary to accurately examine the ability of the model to reproduce the seasonal and high frequency variations of the stratification in the first tens of meters as a good representation of this layer is a challenge for biogeochemical modeling. The high resolution and high frequency meteorological forcing is a major effort of MFSTEP and constitutes an asset for regional modeling especially in the Northern Mediterranean dominated by winds channeled by the orography. The impact of the correct representation of the wind curl enabled by the high resolution modeling was already shown (Estournel et al., 2003). It is likely that the high frequency wind is also beneficial especially in the context of short-term forecasting of currents.

To conclude this scale oriented study of the NWM dynamics, we focused on the regional distribution of dense water in winter and a wind induced upwelling.

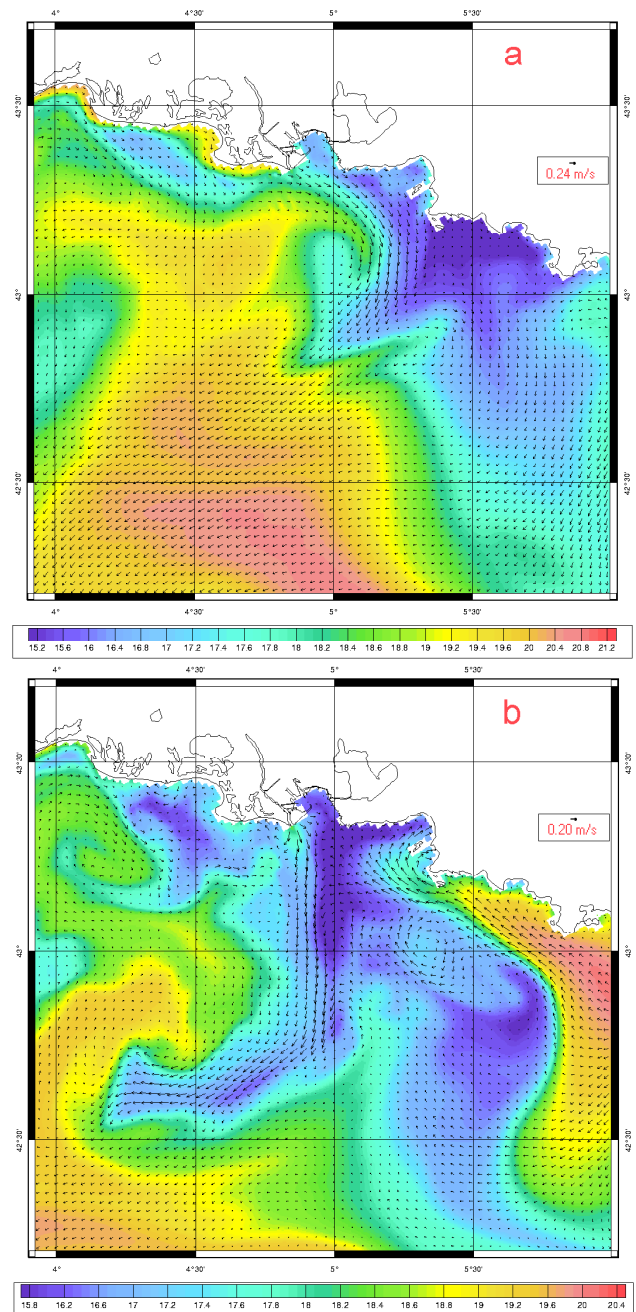


**Fig. 14.** Surface current superimposed on sea surface for (a) 25 September 2004 (b) 29 September 2004.

The regional model allows to represent a number of processes especially those induced by the wind as coastal upwelling under stratified conditions, dense water formation over the Gulf of Lion shelf, deep mixing in the convection zone or influence on the Northern Current penetration in the Gulf of Lion. On the other hand, some doubtful regional features as the circulation in the Catalan Sea should be studied in more detail especially by taking a careful look at available

observations. The increasing volume of data available thanks to MFS should allow us to better understand the major drawbacks of the modeling system and then to contribute to improve it at its different scales.

## Appendix A

### Model equations in sigma coordinate system

Momentum equations under Boussinesq approximation are given by:

$$\frac{\partial \tilde{u}}{\partial t^*} + \frac{\partial \tilde{u}u}{\partial x^*} + \frac{\partial \tilde{v}u}{\partial y^*} + \delta\sigma \frac{\partial \omega u}{\partial \sigma} - f \tilde{v} = \frac{-D}{\rho_0} \frac{\partial p}{\partial x} + \frac{\partial}{\partial x^*} \tilde{K}^x \frac{\partial u}{\partial x^*} + \frac{\partial}{\partial y^*} \tilde{K}^y \frac{\partial u}{\partial y^*} + \frac{\delta\sigma}{h+\eta} \frac{\partial}{\partial \sigma} K^z \frac{\partial u}{\partial \sigma} \quad (A1)$$

$$\frac{\partial \tilde{v}}{\partial t^*} + \frac{\partial \tilde{u}v}{\partial x^*} + \frac{\partial \tilde{v}v}{\partial y^*} + \delta\sigma \frac{\partial \omega v}{\partial \sigma} + f \tilde{u} = \frac{-D}{\rho_0} \frac{\partial p}{\partial y} + \frac{\partial}{\partial x^*} \tilde{K}^x \frac{\partial v}{\partial x^*} + \frac{\partial}{\partial y^*} \tilde{K}^y \frac{\partial v}{\partial y^*} + \frac{\delta\sigma}{h+\eta} \frac{\partial}{\partial \sigma} K^z \frac{\partial v}{\partial \sigma} \quad (A2)$$

The stars indicate that the variables are in the sigma coordinate system and the tilde variables refer to a multiplication by the corresponding layer thickness  $D$  given by  $D=(h+\eta)\delta\sigma$  (e.g.:  $\tilde{u}=Du$ ) where  $h$  is the motionless water depth,  $\eta$  the surface elevation anomaly and  $\delta\sigma$  the sigma increment. The hydrostatic approximation in sigma coordinates, leads to the following formulation of the horizontal pressure gradient:

$$-\frac{1}{\rho_0} \frac{\partial p}{\partial x} = -g \frac{\partial \eta}{\partial x} - \frac{1}{\rho_0} \left( \frac{\partial p'}{\partial x^*} + \frac{\partial z}{\partial x^*} g \rho' \right) \quad (A3)$$

where  $p' = g \int_z^\eta \rho' dz'$  is the hydrostatic pressure associated with the density anomaly:  $\rho' = \rho - \rho_0$ .

Density is related to temperature and salinity via the state equation, and the evolution of temperature and salinity is given by:

$$\frac{\partial \tilde{T}}{\partial t^*} + \frac{\partial \tilde{u}T}{\partial x^*} + \frac{\partial \tilde{v}T}{\partial y^*} + \delta\sigma \frac{\partial \omega T}{\partial \sigma} = \frac{\partial}{\partial x^*} \tilde{K}^x \frac{\partial T}{\partial x^*} + \frac{\partial}{\partial y^*} \tilde{K}^y \frac{\partial T}{\partial y^*} + \frac{\delta\sigma}{h+\eta} \frac{\partial}{\partial \sigma} K^z \frac{\partial T}{\partial \sigma} + \frac{\delta\sigma}{\rho C_p} \frac{\partial Q}{\partial \sigma} \quad (A4)$$

$$\frac{\partial \tilde{S}}{\partial t^*} + \frac{\partial \tilde{u}S}{\partial x^*} + \frac{\partial \tilde{v}S}{\partial y^*} + \delta\sigma \frac{\partial \omega S}{\partial \sigma} = \frac{\partial}{\partial x^*} \tilde{K}^x \frac{\partial S}{\partial x^*} + \frac{\partial}{\partial y^*} \tilde{K}^y \frac{\partial S}{\partial y^*} + \frac{\delta\sigma}{h+\eta} \frac{\partial}{\partial \sigma} K^z \frac{\partial S}{\partial \sigma} \quad (A5)$$

where  $\frac{\partial Q}{\partial \sigma}$  is the solar radiative heat flux forcing. This flux is related to its surface value through a double exponential decrease as stated by Paulson and Simpson (1977):

$$\frac{Q}{Q_s} = 0.42 e^{\frac{\tilde{z}}{23}} + 0.58 e^{\frac{\tilde{z}}{0.35}} \quad (A6)$$

The continuity equation is given by:

$$\frac{\partial \tilde{u}}{\partial x^*} + \frac{\partial \tilde{v}}{\partial y^*} + \delta\sigma \left( \frac{\partial \omega}{\partial \sigma} + \frac{\partial \eta}{\partial t^*} \right) = 0 \quad (A7)$$

In the generalized sigma coordinate system,  $\delta\sigma$  is likely to be a function of the horizontal coordinates  $x$  and  $y$  whereas in the usual “simple” sigma coordinate system  $\delta\sigma$  is a constant of  $x$  and  $y$  but can depend on the vertical coordinate leading to a higher vertical resolution near the bottom or the surface. In this latter case, the above equations are similar to the classical sigma coordinate equations. When  $\delta\sigma$  is independent of the horizontal coordinate, the continuity Eq. (A7) leads for instance to:

$$\frac{\partial(h+\eta)u}{\partial x^*} + \frac{\partial(h+\eta)v}{\partial y^*} + \frac{\partial\omega}{\partial\sigma} + \frac{\partial\eta}{\partial t^*} = 0 \quad (A8)$$

## Appendix B

### Expression of surface momentum and heat fluxes

The momentum and turbulent heat fluxes are computed following:

$$\begin{aligned} E &= \rho_a C_E (q_{2m} - q_{0m}^{\text{sat}}) |U_{10m}| \\ Q_H &= \rho_a C_P (\theta_{2m} - T_{0m}) |U_{10m}| \\ \tau &= \rho_a C_D |U_{10m}| U_{10m} \end{aligned} \quad (B1)$$

where  $U_{10m}$  is the 10 m high wind,  $q_{2m}$  and  $\theta_{2m}$  are respectively the air specific humidity and the potential temperature in Kelvin at 2 m high above sea surface,  $\rho_a \approx 1.226 \text{ kg m}^{-3}$  is the reference air density and  $T_{0m}$  the sea surface temperature in Celsius. The air at the surface is assumed to be saturated, with a specific humidity deduced from saturated vapor pressure ( $p_{vs}$ ), saturation mixing ratio ( $r$ ) and surface atmospheric pressure ( $p_{0m}$ ):

$$\begin{aligned} q_{0m}^{\text{sat}} &= 0.98 r / (1 + r) \\ r &= 0.622 p_{vs} / (p_{0m} - p_{vs}) \\ p_{vs} &= 610.78 e^{\frac{17.27 T_{0m}}{T_{0m} + 237.29}} \end{aligned} \quad (B2)$$

The drag coefficient ( $C_D$ ) and the transfer coefficient for evaporation ( $C_E$ ) and sensible heat ( $C_H$ ) are functions of atmospheric stability ( $\zeta$ ) and wind speed. Their neutral stability values, used to start the iterative procedure, are given by:

$$\begin{aligned} C_{DN} &= \max(0.93 \times 10^{-3}, 0.61 \times 10^{-3} \\ &\quad + 6.3 \times 10^{-5} |U_{10m}|) \\ C_{EN} &= 1.2 \times 10^{-3} \\ C_{HN} &= 0.7 \times 10^{-3} \text{ stable } \zeta > 0 \\ C_{HN} &= 1.2 \times 10^{-3} \text{ unstable } \zeta \leq 0 \end{aligned} \quad (B3)$$

with

$$\zeta(z) = \frac{g k z t^* (1 + 0.608 q_{10m}) + q^* 0.608 \theta_{10m}}{u^{*2} \theta_{10m} (1 + 0.608 q_{10m})} \quad (B4)$$

where  $k=0.4$  is the von Karman constant, and  $u^*$ ,  $t^*$ ,  $q^*$ , the turbulent scales given by:

$$\begin{aligned} u^* &= \sqrt{C_D} U_{10m} \\ t^* &= C_H U_{10m} \frac{\theta_{10m} - (T_{0m} + 273.15) \left(\frac{10^5}{p_{0m}}\right)^{0.286}}{u^*} \\ q^* &= C_E U_{10m} \frac{q_{10m} - q_{0m}^{sat}}{u^*} \end{aligned} \quad (B5)$$

In this expression, the 10 m height values have been deduced from the 2m ones according to:

$$\begin{aligned} q_{10m} &= q_{2m} + \frac{q^*}{k} \left( \ln\left(\frac{10}{2}\right) - \varphi(\zeta_{10m}) + \varphi(\zeta_{2m}) \right) \\ \theta_{10m} &= \theta_{2m} + \frac{t^*}{k} \left( \ln\left(\frac{10}{2}\right) - \varphi(\zeta_{10m}) + \varphi(\zeta_{2m}) \right) \end{aligned} \quad (B6)$$

The functions  $\varphi_m(\zeta)$  and  $\varphi_h(\zeta)$  are given by:

$$\begin{aligned} \varphi_m(\zeta) &= \varphi_h(\zeta) = -7\zeta \text{ stable}, \zeta \geq 0 \\ \varphi_m(\zeta) &= 2 \ln\left(\frac{1+X}{2}\right) + \ln\left(\frac{1+X^2}{2}\right) - 2 \tan^{-1}(X) + \frac{\pi}{2} \\ &\quad \text{unstable}, \zeta < 0 \\ \varphi_h(\zeta) &= 2 \ln\left(\frac{1+X^2}{2}\right) \text{ unstable}, \zeta < 0 \\ X &= (1 - 16\zeta)^{1/4} \end{aligned} \quad (B7)$$

and  $C_D$ ,  $C_E$ ,  $C_H$  are eventually given by:

$$\begin{aligned} C_D &= C_{DN} \left( 1 - \frac{\sqrt{C_{DN}}}{k\varphi_m(\zeta_{10m})^2} \right) \\ C_H &= C_{HN} \sqrt{\frac{C_D}{C_{DN}}} \left( 1 - \frac{C_{HN}}{k\sqrt{C_{DN}\varphi_h(\zeta_{10m})}} \right) \\ C_E &= C_{EN} \sqrt{\frac{C_D}{C_{DN}}} \left( 1 - \frac{C_{EN}}{k\sqrt{C_{DN}\varphi_h(\zeta_{10m})}} \right) \end{aligned} \quad (B8)$$

Edited by: N. Pinardi

## References

- Auclair, F., Marsaleix, P., and Estournel, C.: Sigma coordinate pressure gradient errors : evaluation and reduction by an inverse method, *J. Atmos. Ocean. Tech.*, 17, 1348–1367, 2000a.
- Auclair, F., Casitas, S., and Marsaleix, P.: Application of an inverse method to coastal modelling, *J. Atmos. Ocean. Tech.*, 17, 1368–1391, 2000b.
- Auclair, F., Marsaleix, P., and Estournel, C.: The penetration of the Northern Current over the Gulf of Lion (western Mediterranean Sea) as a downscaling problem, *Oceanol. Acta*, 24, 529–544, 2001.
- Auclair, F., Estournel, C., Marsaleix, P., and Pairaud, I.: On coastal ocean embedded modelling, *Geophys. Res. Lett.*, 33, L14602, doi:10.1029/2006GL026099, 2006.
- Blumberg, A. F. and Mellor, G. L.: A description of a three-dimensional coastal circulation model, in: *Three-Dimensional Coastal Ocean Models*, edited by: Heaps, N., Coastal Estuarine Sci., Vol. 4, AGU, Washington, DC, 1–16, 1987.
- Brožková, R., Derková, M., Belluš, M., and Farda, A.: Atmospheric forcing by ALADIN/MFSTEP and MFSTEP oriented tunings, *Ocean Sci.*, 2, 113–121, 2006, <http://www.ocean-sci.net/2/113/2006/>.
- Demirov, E. and Pinardi, N.: The Simulation of the Mediterranean Sea circulation from 1979 to 1993: Part I. The interannual variability, *J. Marine Syst.*, 33–34, 23–50, 2002.
- Dufau-Julliand, C., Marsaleix, P., Petrenko, A., and Dekeyser, I.: Three-dimensional modeling of the Gulf of Lion's hydrodynamics (northwest Mediterranean) during January 1999 (MOOGLI3 Experiment) and late winter 1999: Western Mediterranean Intermediate Water's (WIW's) formation and its cascading over the shelf break, *J. Geophys. Res.*, 109, C11002, doi:10.1029/2003JC002019, 2004.
- Emelianov, M., Font, J., Turiel, A., Millot, C., Solé, J., Poulain, P.-M., Julià, A., and Vitrià, M.-R.: Transformation of Levantine Intermediate Water tracked by MEDARGO floats in the Western Mediterranean, *Ocean Sci.*, 2, 281–290, 2006, <http://www.ocean-sci.net/2/281/2006/>.
- Estournel, C., Kondrachoff, V., Marsaleix, P., and Vehil, R.: The plume of the Rhône: numerical simulation and remote sensing, *Cont. Shelf Res.*, 17, 899–924, 1997.
- Estournel, C., Broche, P., Marsaleix, P., Devenon, J. L., Auclair, F., and Vehil, R.: The Rhone river plume in unsteady conditions: numerical and experimental results, *Estuar. Coast. Shelf Sci.*, 53, 25–38, 2001.
- Estournel, C., Durrieu de Madron, X., Marsaleix, P., Auclair, F., Julliand, C., and Vehil, R.: Observation and modelisation of the winter coastal oceanic circulation in the Gulf of Lions under wind conditions influenced by the continental orography (FETCH experiment), *J. Geophys. Res.*, 108(C3), 7.1–7.18, 2003.
- Gaspar, P., Grégoris, Y., and Lefevre, J. M.: A simple eddy kinetic energy model for simulations of the oceanic vertical mixing: tests at station Papa and long-term upper ocean study site, *J. Geophys. Res.*, 95, 179–193, 1990.
- Gatti, J.: Intrusions du Courant Nord Méditerranéen sur la partie est du plateau continental du Golfe du Lion, Ph.D. thesis, Université de la Méditerranée, 2008.
- Geernaert, G. L.: Bulk parameterizations for the wind stress and heat fluxes, in: *Surface waves and fluxes*, edited by: Geernaert, G. L. and Plant, W. J., I, 91–192, 1990.
- Georgelin, M. and Richard, E.: Numerical simulation of flow diversion around the Pyrenees: A tramontana case study, *Mon. Weather Rev.*, 124, 687–700, 1996.
- Guizien, K., Brochier, T., Duchêne, J.-C., Koh, B.-S., and Marsaleix, P.: Dispersal of *owenia fusiformis* larvae by wind-driven currents: turbulence, swimming behaviour and mortality in a three-dimensional stochastic model, *Mar. Ecol.-Prog. Ser.*, 311, 47–66, 2006.
- Haney, R. L.: On the Pressure Gradient Force over Steep Topography in Sigma Coordinate Ocean Models, *J. Phys. Oceanogr.*, 21, 610–619, 1991.
- Johns, B., Marsaleix, P., Estournel, C., and Vehil, R.: On the wind-driven upwelling circulation in the Gulf of Lions, *J. Marine Syst.*, 3, 309–320, 1992.
- Jorda Sanchez, G.: Towards data assimilation in the Catalan continental shelf – From data analysis to optimization methods, Ph.D. thesis, University of Barcelona, 280 pp., 2005.

- Leitão, P., Coelho, H., Santos, A., and Neves, R.: Modeling the main features of the Algarve coastal circulation during July 2004: a downscaling approach, *Journal of Atmospheric and Ocean Science*, 10, 421–462, 2007.
- Leredde, Y., Denamiel, C., Brambilla, E., Bouchette, F., Lauer-Leredde, C., and Marsaleix, P.: Hydrodynamics in the Gulf of Aigues-Mortes, NW Mediterranean Sea: *in situ* and modelling data, *Cont. Shelf Res.*, 27, 2389–2406, 2007.
- Lopez-Jurado, J.-L., Gonzalez-Pola, C., and Velez-Belchi, P.: Observation of an abrupt disruption of the long-term warming trend at the Balearic Sea, western Mediterranean Sea, in summer 2005, *Geophys. Res. Lett.*, 32, L24606, doi:10.1029/2005GL024430, 2005.
- Marsaleix, P., Estournel, C., Kondrachoff, V., and Vehil, R.: A numerical study of the formation of the Rhone river plume, *J. Marine Syst.*, 14, 99–115, 1998.
- Marsaleix, P., Auclair, F., and Estournel, C.: Considerations on open boundary conditions for regional and coastal ocean models, *J. Atmos. Ocean. Tech.*, 23, 1604–1613, 2006.
- Marsaleix, P., Auclair, F., Floor, J. W., Herrmann, M. J., Estournel, C., Pairaud, I., and Ulses, C.: Energy conservation issues in sigma-coordinate free-surface ocean models, *Ocean Model.*, 20, 61–89, 2008.
- Marullo, S., Buongiorno Nardelli, B., Guarracino, M., and Santoleri, R.: Observing the Mediterranean Sea from space: 21 years of Pathfinder-AVHRR sea surface temperatures (1985 to 2005): re-analysis and validation, *Ocean Sci.*, 3, 299–310, 2007, <http://www.ocean-sci.net/3/299/2007/>.
- Millot, C.: The Gulf of Lions' hydrodynamics, *Cont. Shelf Res.*, 10(9–11), 885–894, 1990.
- Paulson, C. A. and Simpson, J. J.: Irradiance Measurements in the upper ocean, *J. Phys. Oceanogr.*, 7, 952–956, 1977.
- Petrenko, A., Leredde, Y., and Marsaleix, P.: Circulation in a stratified and wind-forced Gulf of Lions, NW Mediterranean Sea: *in situ* and modeling data, *Cont. Shelf Res.*, 25, 7–27, 2005.
- Pietrzak, J., Jakobson, J. B., Burchard, H., Vested, H. J., and Petersen, O.: A three-dimensional hydrostatic model for coastal and ocean modelling using a generalised topography following co-ordinate system, *Ocean Model.*, 4, 173–205, 2002.
- Pinardi, N., Auclair, F., Cesarini, C., Demirov, E., Fonda-Umani, S., Giani, M., Montanari, G., Oddo, P., Tonani, M., and Zavatarelli, M.: Toward marine environmental prediction in the Mediterranean Sea coastal areas: a monitoring approach, in: *Ocean Forecasting: conceptual basis and applications*, edited by: Pinardi, N., Springer Verlag, 339–373, 2001.
- Reffray, G., Fraunié, P., and Marsaleix, P.: Secondary flows induced by wind forcing in the Rhône region of freshwater influence, *Ocean Dynam.*, 54, 179–196, 2004.
- Tonani, M., Pinardi, N., Fratianni, C., and Dobricic, S.: Forecast and analysis assessment through skill scores, *Ocean Sci. Discuss.*, 4, 189–212, 2007, <http://www.ocean-sci-discuss.net/4/189/2007/>.
- Tonani, M., Pinardi, N., Dobricic, S., Pujol, I., and Fratianni, C.: A high-resolution free-surface model of the Mediterranean Sea, *Ocean Sci.*, 4, 1–14, 2008, <http://www.ocean-sci.net/4/1/2008/>.
- Ulses, C., Grenz, C., Marsaleix, P., Schaaff, E., Estournel, C., Meulé, S., and Pinazo, C.: Circulation in a semi enclosed bay under the influence of strong fresh water input, *J. Marine Syst.*, 56, 113–132, 2005.